RSC Advances

PAPER

View Article Online
View Journal | View Issue



Cite this: *RSC Adv.*, 2014, **4**, 62393

# Fabrication of gold/polypyrrole core/shell nanowires on a flexible substrate for molecular imprinted electrochemical sensors†

Wei-Ren Huang,[a] Yu-Liang Chen,[a] Chi-Young Lee[b] and Hsin-Tien Chiu*[a]

Received 4th October 2014
Accepted 12th November 2014

DOI: 10.1039/c4ra11774c

www.rsc.org/advances

In this work, we fabricated gold-nanowires (Au NWs) on flexible substrates by direct current electrochemical deposition. Then, we electropolymerized a polypyrrole layer onto the Au NWs *via* cyclic voltammetry (CV) as the molecular imprinted polymer biosensor to detect dopamine (DA). The influence of the scan rate of CV for the sensor preparation was optimized. CV and differential pulse voltammetry (DPV) were used to measure different DA concentrations. The Au/polypyrrole core/shell nanowires sensor showed good DPV signal intensity at 805 μA $mM^{-1}$ and the determined linear range for DA was $4 \times 10^{-7}$ to $1 \times 10^{-5}$ M ($N = 3$).

## Introduction

Biosensors play important roles nowadays. They are widely used in food safety monitoring, environmental pollution control, disease diagnosis, and medical care.[1–8] Sensitivity and specificity are critical issues for biosensors to offer correct results. To enhance specificity, antibody, enzyme, and aptamer modifications on the surface of sensors are common.[9–14] However, they are a high price because of their complex fabrication process and low storage temperature. On the other hand, molecular imprinted polymers (MIPs) are attractive alternatives for biosensors because their preparation is simple and low cost.[15–18] In addition, they offer good physical and chemical stability and durability.[16,17] Molecular imprinting techniques prepare polymer scaffolds that function as synthetic receptors. These receptors can generate significant electrochemical signal intensity differences between the binding and the extraction of the target molecules. Specificity of MIPs is provided during polymerization of monomers in the presence of template molecules. Subsequent removal of the molecules leaves empty binding sites complementary in size and shape to these target molecules. Therefore, these sites can recognize the targets and rebind them based on many intermolecular forces.[19–23] Conducting polymers such as polypyrrole (PPy) and polyaniline are widely applied to the fabrication of MIPs sensors.[24–26] They are easy to synthesize and provide good electron transfer signals.[26,27]

Dopamine (DA) is one of the important neurotransmitters in the brain and the central nervous system. DA is well known for regulating many physiological properties, including behavior, movement, endocrine, and cardiovascular, renal and gastrointestinal functions.[33] Previous studies reveal that the DA concentration is critical to nervous diseases such schizophrenia, Parkinson's disease and HIV.[34–37] Therefore, rapid, cheap and sensitive detections of the DA concentration *in vivo*/*vitro* is critical. Recently, MIP sensors composed of nanomaterials (carbon nanotubes (CNTs), noble metal nanoparticles and nanostructures) modified conventional electrodes (glassy carbon, Au and Pt) showed much improved sensing performances.[16,28–32] This is due to their increased surface areas which allow the formation of more receptors. Consequently, the sensitivities and the detection ranges are enhanced. The usefulness of the sensors may be enhanced further by growing the sensing materials on flexible substrates.[38–40] They show many advantages over hard ones. These frequently include thinness, light weight, high portability, and resistance to mechanical damages. Previously, We have demonstrated that with proper aptamer modification of the Au surface, Au nanowires (NWs) electrochemically deposited on flexible polyethylene terephthalate (PET) substrate (Au NW/PET) can function as an efficient electrochemical protein sensor.[41] In addition, without any modification, Au NW/PET can be employed as a biosensor to detect DA electrochemically.[42] In order to increase the selectivity of the Au NW/PET electrode, in this work, we report the development of a MIP modified Au NW/PET sensor for efficient DA detection. PPy is electrochemically polymerized on the surface of the NW so that an Au NW/PPy core/shell structure is formed. We discuss our observations below.

[a]*Department of Applied Chemistry, National Chiao Tung University, Hsinchu, Taiwan 30010, Republic of China. E-mail: htchiu@nctu.edu.tw*

[b]*Department of Materials Science and Engineering, National Tsing Hua University, Hsinchu, Taiwan 30013, Republic of China*

† Electronic supplementary information (ESI) available: Fabrication steps for conductive substrates, electrochemical deposition system for Au NW growth, CVs for electrode fabrications, EDS, SEM, TEM, and DPV data. See DOI: 10.1039/c4ra11774c

# Experimental section

### Chemicals and instruments

Hydrogen tetrachloroaurate(III) ($HAuCl_4 \cdot 3H_2O$, 99%), phosphate dibasic dihydrate ($Na_2HPO_4 \cdot 2H_2O$, 99.5%), pyrrole ($C_4H_4NH$, 98%), sodium perchlorate ($NaClO_4$, >98%), D-(+)-glucose ($C_6H_{12}O_6$, >99.5%), dopamine hydrochloride (DA HCl), uric acid (UA), ascorbic acid (AA), and catechol (CA) (>99%) were purchased from Sigma Aldrich. Cetyltrimethylammonium chloride (CTAC, purity: 890 mM) was supplied by Taiwan Surfactant. Sodium nitrate ($NaNO_3$, 99.9%) was provided by Riedel-de Haën. Sodium phosphate ($NaH_2PO_4 \cdot H_2O$, 99.6%) was bought from J.T. Baker. The as-received chemical were analytical grade and used without further purification. Deionized (DI) water Milli-Q grade, >18 M was used throughout the fabrication. PET substrates were acquired from Schmidt Film and cut and cleaned before further processing.

Scanning electron microscopic (SEM) images and energy dispersive spectroscopic (EDS) data were taken from a Hitachi S-4000 (25 keV) and JEOL JIM-7401F (15 keV). Transmission electron microscopic (TEM) images were obtained from a JEOL JEM-2010 (200 keV). Raman spectra were gained from a high resolution confocal Raman microscope (HOROBA, Lab RAM HR). Cyclic voltammetry (CV) measurements were performed by a CH Instruments electrochemical potentiostat (CHI 6081C). Differential pulse voltammetry (DPV) measurements were performed on an Autolab PGSTAT30.

### Fabrication of Au nanowires on PET substrates

Ti (150 nm) and Au (100 nm) thin layers were grown on transparent PET substrates by an e-gun evaporation system (ULVAC EBX-8C). The fabrication steps for the conductive substrates are shown in Fig. S1 in the ESI.† Each of the Au film on PET (Au/PET) substrates was further masked by Kapton tapes so that the exposed surface was 0.5 cm × 0.5 cm. They were employed to fabricate all the electrodes investigated in this article. Au NWs were electrochemically grown the PET substrates (cathode) with a direct current (DC) power supply Twintek TP1818 (Fig. S2 in ESI†) operated at 298 K and 0.7 V.[41] A dried carbon paste on a PET transparency was used as the anode. The electroplating solution contained $HAuCl_{4(aq)}$ (5 mM), $CTAC_{(aq)}$ (10 mM) and $NaNO_{3(aq)}$ (20 mM) in DI water. After the as-prepared Au NW/PET electrodes were washed with alcohol (Sigma Aldrich, 97%) and DI water, they were dried in a steam of $N_{2(g)}$. The electrodes were stored at the ambient temperature.

### Fabrication of Au/PPy core/shell nanowire (APPW) and Au/PPy film (APPF) electrodes

In a solution composed of $NaClO_{4(aq)}$ (100 mM), $DA_{(aq)}$ (20 mM), and $pyrrole_{(aq)}$ (50 mM), PPy was electropolymerized according to a previously published CV process on the as-prepared Au NW/PET substrates to form Au/PPy core/shell nanowire (APPW) electrodes.[43] By employing CV scans (7 cycles, −0.8, −1.0 V, scan rates 100–900 mV $s^{-1}$), corresponding electrodes APPW100–APPW900 were fabricated. The electrodes were rinsed with DI water, dried in a stream of $N_{2(g)}$, and stored in the ambient environment.

In addition, by using the same process with a scan rate 500 mV $s^{-1}$, a PPy film was electropolymerized on an Au/PET substrate to offer an Au/PPy film electrode APPF500.

An Au/PPy core/shell nanowire electrode fabricated at a scan rate 500 mV $s^{-1}$ without the presence of DA was designated as APPW500N. The DA molecules trapped inside the PPy layers in APPW100–APPW900 and APPF500 were removed by CV scans before the electrochemical measurements of DA (see below). After DA molecules were extracted, corresponding APPW100E–APPW900E and APPF500E electrodes were obtained.

### Electrochemical measurements of DA

A three-electrode system was used for all electrochemical measurements. The system contained an APPW or an APPF electrode (0.5 cm × 0.5 cm) as the working electrode, a Pt wire as the counter electrode, and an Ag/AgCl half-cell (in KCl 3.0 M) as the reference electrode. To remove DA in the PPy layer on the as-fabricated electrodes, CV scans (10 cycles, −0.2, −0.6 V, scan rate 100 mV $s^{-1}$) were carried out to oxidize DA into the quinone form.[43] Through the process, electrodes APPW100E–APPW900E and APPF500E were fabricated prior to the further DA detections. To detect the oxidation current of DA, differential pulse voltammetric (DPV) measurements were performed so that the charging currents could be minimized.[44] The electrode was immersed in a DA containing phosphate buffered saline (PBS, 0.1 M, pH 7.4) solution for 25 min. DPV measurements (−0.2 to −0.4 V) were carried out in the PBS too.

# Results and discussion

### Preparation and characterization of APPWs

As shown in the scheme in Fig. 1, pyrrole molecules are electropolymerized on Au NW/PET substrates to form APPW electrodes. Fig. S3 in ESI† shows the CV scans employed during the

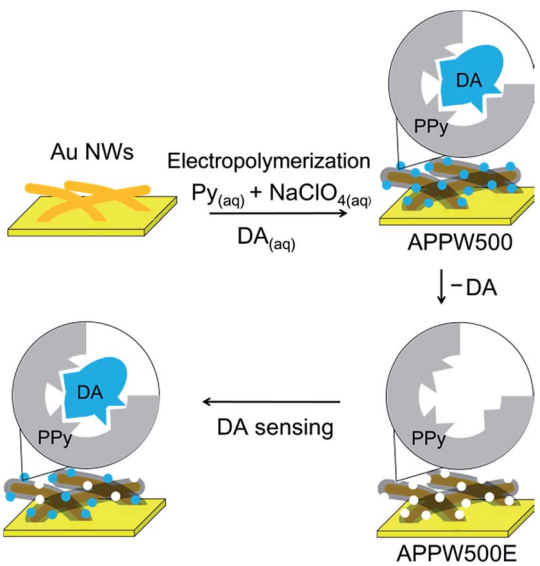


Fig. 1 Synthetic process of DA imprinted PPy polymer on Au NW/PET substrate for DA sensing.

 

preparations of APPW500 and APPW500N. The former shows an obvious peak at 0.162 V in the first cycle. This is assigned to the oxidation of DA to the quinone form.[43] The anodic peak at 0.9 V is due to oxidation of Py to its radical cation and formation of PPy.[45] In addition, the increased broad anodic peaks at 0.150 V and the cathodic peaks at 0.00 V are due to the PPy growth.[46]

SEM and TEM images of APPW500 are displayed in Fig. 2. As shown in Fig. 2A, the as-fabricated Au/PPy core/shell NWs are 90–200 nm wide and 10–20 μm long. In Fig. 2B, the image of an NW in APPW500 suggests that the thickness of the shell layer is $22.4 \pm 3.8$ nm. The EDS signals of the light elements C, N, and O from an as-prepared Au NW/PET substrate (Fig. S4 in ESI†) enhance significantly after the PPy layer was grown on it to provide the APPW500 sample (Fig. 2C). Clearly, the C and N signals are attributed to the PPy layers and the incorporated DA molecules. The O signal is assigned to DA molecules and $ClO_4^-$ ions trapped inside PPy during the electropolymerization process.

The Raman spectra of APPW500, APPW500E (APPW500 after extracting), and APPW500N are shown in Fig. 2D. APPW500N displays six main bands at 1590, 1414, 1335, 1046, 988, and 923 $cm^{-1}$. The strong band at 1590 $cm^{-1}$ is assigned to the PPy C=C backbone stretching of PPy while the moderate bands at 1414 and 1335 $cm^{-1}$ are correlated to the ring stretching and the C=C in-plane deformation. The weak bands at 1046, 988, and 923 $cm^{-1}$ are attributed to the C–H in-plane deformations. The spectrum of APPW500E closely resembles that of APPW500N. On the other hand, APPW500 displays two additional bands at 1493 and 1261 $cm^{-1}$. They are associated with the C–O stretching and the ring vibration from the catechol substructure in the templating DA.[47,48] The results are in good agreement with the fabrication processes of the samples. They indicate that the surface of APPW500 is composed of both PPy and DA while APPW500N and APPW500E are essentially DA free.

In this study, the CV scan rates of the electropolymerization process affect the PPy layer thicknesses significantly. In Fig. S5 in ESI,† the SEM images of the samples prepared at different scan rates are presented. The NW surfaces are smooth before the electropolymerization (Fig. S6A). As the scan rates decrease, the PPy layers on the APPW electrodes become rough and interconnected (Fig. S5B–F†). In addition, the TEM images in Fig. S6† also reveal that the scan rates control the PPy layer thicknesses. They increase from 3 nm to 168 nm as the scan rates decrease from 900 mV $s^{-1}$ to 100 mV $s^{-1}$.

After the removal of the DA template molecules from APPW100–APPW900, the as-obtained electrodes were investigated by DPV to understand their responses to a DA solution. Fig. 3A shows the DPV signals of APPW100E–APPW900E in a DA ($10^{-4}$ M) containing PBS (0.1 M, pH 7.4). In Fig. 3B, intensities from the DPV scans at 0.157 V and the corresponding PPy layer thicknesses are plotted against the synthetic CV scan rates of PPy. Although the PPy layer thickness is comparatively thin, APPW500E shows the strongest DPV signal intensity. We suggest that when the PPy layer is thin, it does not provide enough DA recognition sites. On the other hand, when the PPy layer is thick and interconnected, only a small portion of the DA recognition sites is occupied because the diffusion of DA deep into the thick layer becomes more difficult. In addition, the electron transfer through the thick layer becomes difficult too. As a result, the DPV signal intensity diminishes as well.

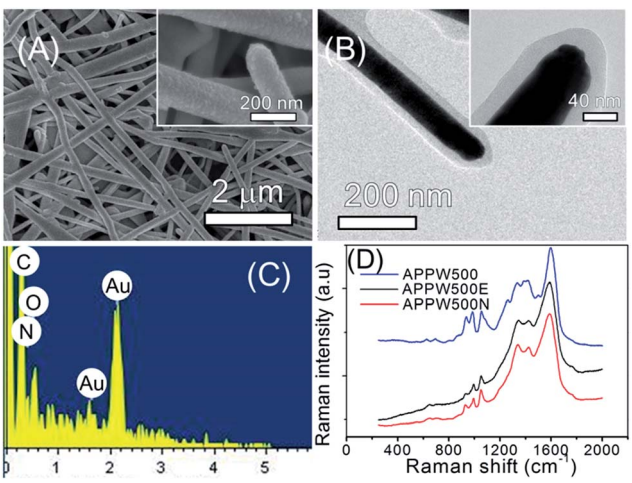


Fig. 2 (A) Low and high magnification (inset) SEM images, (B) low and high magnification (inset) TEM images and (C) EDS of APPW500. (D) Raman spectra of APPW500 (blue line), APPW500E (black line) and APPW500N (red line).

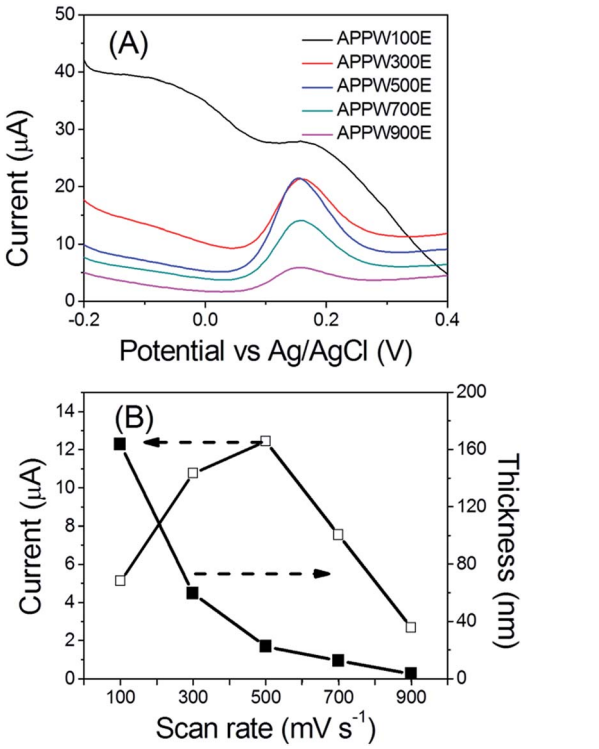


Fig. 3 (A) Plots of DPV responses with different synthesis scan rates in DA ($10^{-4}$ M, in PBS). (B) Plots of DPV signal intensities of DA ($10^{-4}$ M, in PBS) (□) and thicknesses of PPy layers (■) against synthetic CV scan rates of electrodes.

Consequently, we choose the best performed APPW500E electrode for further investigations.

### DPV responses of DA on APPF500E, APPW500N, APPW500E and Au NWs

Fig. 4A presents the DPV signals of APPF500E, APPW500N, APPW500E, and plain Au NWs to DA ($10^{-4}$ M). As shown by the results, APPW500E demonstrates the strongest intensity than the others do. Fig. 4B displays the signal intensities of the four electrodes at 0.157 V. APPW500E shows the highest signal intensity than the other electrodes do. The electrode provides more DA recognizing sites due to the molecular-imprinted PPy layer and the high surface area NWs. In contrast, APPW500N (electropolymerized without the presence of DA) can only generate a weak DA oxidation current. It cannot trap DA molecules due to the lack of the recognition sites. APPF500E is composed of a thin PPy film on an Au thin film substrate. It does not provide surface area as high as the NWs. Thus, the signal is weak. For the Au NW electrode, although it has a high surface area, it is not able to capture DA because of the absence of the MIP layer.

### Performance of DA detection by APPW500E

Fig. 5A presents the DPV responses of APPW500E after incubated in PBS solutions (pH 7.4) with different DA concentrations. Clearly, as the concentration increases, the DA oxidation peak intensity increases as well. As displayed in Fig. 5B, the linear range of DA concentration is 0.4–10 μM with a relation coefficient 0.9952 ($N = 3$). By using the linear regression equation I (μA) = 0.804$C$ (μM) − 0.198, the sensitivity of APPW500E is estimated to be 805 μA $mM^{-1}$. Table 1 compares the APPW500E performance with those of the other related MIP examples published in literature. While the detection range and the limit of detection (LOD) of the electrode are comparable, its sensitivity is much superior to the other cases.[44,49–52] We attribute this to the high conductivity and the high surface area provided by the Au NWs on the electrode.

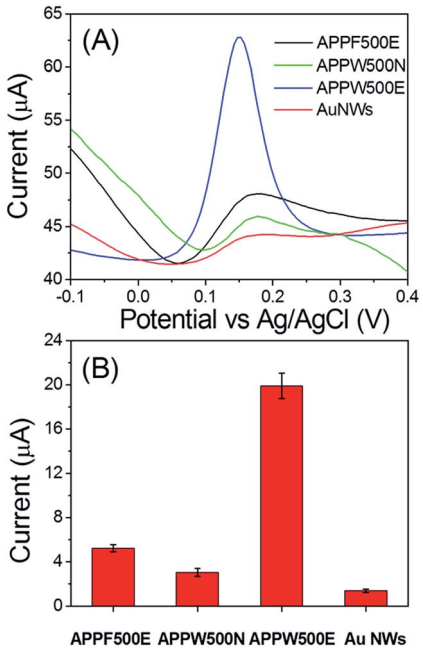


Fig. 4 (A) Plots of DPV responses and (B) signal intensities in DA ($10^{-4}$ M) on APPF500E, APPW500N, APPW500E and Au NWs.

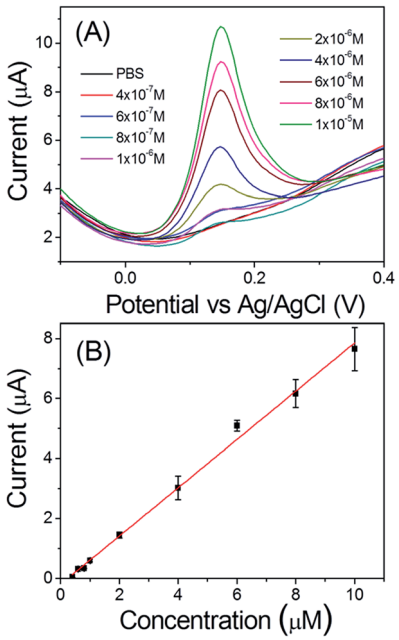


Fig. 5 (A) Plots of DPV responses and (B) calibration curve of DA (0.4–10 μM) on APPW500E.

### Interference studies of DA detection by APPW500E

To understand if APPW500E may distinguish molecules with similar structures, catechol (CA, 1 mM) was chosen as the structure analogue. In addition, ascorbic acid (AA, 1 mM), uric acid (UA, 1 mM), and glucose (G, 1 mM), the molecules in the serum and urine, were mixed with CA as the coexisting interferences. The DPV responses of DA ($10^{-4}$M) and the interfering molecules were measured individually. Then, all of them were mixed and examined by DPV too. Fig. 6 reveals the DPV responses (Fig. 6A) and the signal intensities at 0.157 V (Fig. 6B) of the interfering molecules. Although CA has a structure and an oxidation potential similar and to those of DA, the oxidation current intensity of CA is much lower than that of DA because CA cannot bind to the sites tightly. The oxidation current intensities of UA, G, and AA are small also. They are not able to be trapped in the sites in PPy because of their different structures.[53] In the mixture test, the oxidation current of DA maintains at about 90% of the DA-only signal intensity.

### Durability, stability and homogeneity tests of APPW500E

According to previous studies, MIP electrodes could maintain the performance after chemical treatments.[17] In a durability test, an APPW500E electrode was immersed in $H_2SO_{4(aq)}$ (1 M) first, then in $NaOH_{(aq)}$ (1 M) for 10 min each before a measurement of DA ($10^{-5}$ M) by DPV was carried out. Fig. S7 in

 

Table 1 Comparison of DA detection performance of APPWE500 with other reported MIPs using electrochemical methods

| Electrodes | Method | Detection range (M) | LOD[a] (nM) | Sensitivity (μA $mM^{-1}$) | Ref. |
|---|---|---|---|---|---|
| CNT/PP film | DPV | $6.25 \times 10^{-7}$–$1 \times 10^{-4}$ | 60 | 86 | 44 |
| GSCR/graphene[b] | Amperometry | $1.0 \times 10^{-7}$–$8.3 \times 10^{-4}$ | 100 | 25 | 49 |
| GO-$SiO_2$/MAPSGCE[c] | Amperometry | $5.0 \times 10^{-8}$–$1.6 \times 10^{-4}$ | 60 | 4 | 50 |
| APTES-ITO[d] | CV | $2.0 \times 10^{-6}$–$8.0 \times 10^{-3}$ | — | 41 | 51 |
| POPA-Au film[e] | DPV | $5.0 \times 10^{-7}$–$4.0 \times 10^{-5}$ | 130 | 38 | 52 |
| APPWE500 | DPV | $4.0 \times 10^{-7}$–$1.0 \times 10^{-5}$ | 248 | 805 | This work |

[a] Limit of detection, estimated from three times the standard deviation of the experimental data. [b] GSCR: graphene sheets/Congo red-molecular imprinted polymers. [c] MAPS-GCE: methacryloxypropyl trimethoxysilane and glassy carbon electrode. [d] APTES-ITO: aminopropyl-derivatized organosilane aminopropyltriethoxysilane and indium tin oxide. [e] POPA: poly-*o*-aminophenol.

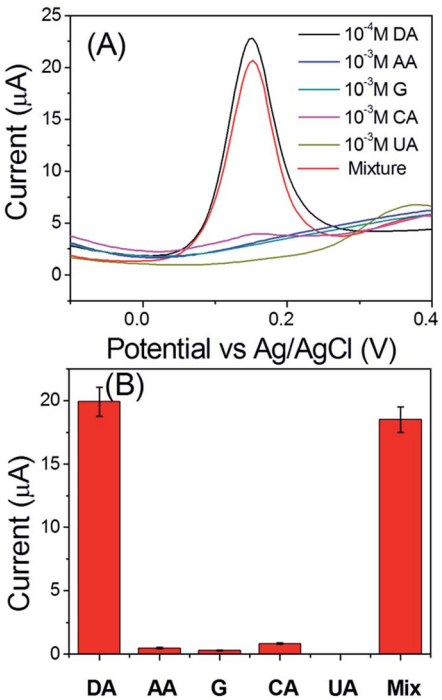


Fig. 6 Interference studies. (A) Plots of DPV responses and (B) signal intensities of UA ($10^{-3}$ M), AA ($10^{-3}$ M), CA ($10^{-3}$ M), G ($10^{-3}$ M), DA ($10^{-4}$ M), and their mixture.

ESI† shows the DPV responses and the signal intensities of the as-prepared APPW500E, after treated in acid, and after treated in base. The oxidation currents generated by the acid and base sequentially treated electrode keeps more than 90% of the original intensity of APPW500E.

In the stability test, an APPW500E electrode was stored and employed to measure DA ($10^{-5}$ M) every 5 days in the ambient environment. Fig. 7 reveals the current retention (%) results from the experiments. After 16 days, the electrode still retained more than 90% of the original current intensity. In the homogeneity test, we used three different APPW500E electrodes to detect DA ($10^{-4}$ M) 2 and 6 days after the fabrication. The current intensities presented in Fig. S8 in ESI† demonstrates very similar values. These results indicate that APPW500E can be preserved easily, endure acidic and basic conditions, and provide excellent reproducibility.

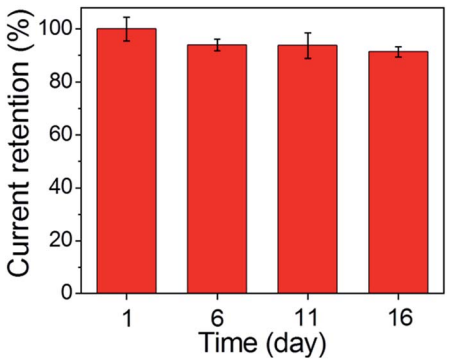


Fig. 7 Storage stability of APPW500E sensor in 16 days ($n = 3$).

## Conclusions

In summary, we have fabricated the MIP electrodes composed of Au/PPy core/shell NWs grown on flexible PET substrates as the electrochemical DA sensor. The thickness of the PPy layer can be controlled *via* controlling the electropolymerization scan rate. Through the simple low cost process, the APPW500E electrode is obtained. It provides a good sensitivity 805 μA $mM^{-1}$ while its linear range is 0.4–10 μM. Additionally, APPW500E demonstrates great DA selectivity when mixed with several interfering molecules. It also maintains 90% DA signal intensity after stored at the ambient environment for 16 days and after acid and base treatments. We anticipate the MIP electrodes will find many sensing applications.

## Acknowledgements

We are grateful to the supports from the National Science Council, "Aim for the Top University Plan" of the National Chiao Tung University, and the Ministry of Education of Taiwan, the Republic of China.

## Notes and references

1 S. Demirci Uzun, F. Kayaci, T. Uyar, S. Timur and L. Toppare, *ACS Appl. Mater. Interfaces*, 2014, **6**, 5235–5243.
2 W. Wu, Z. Fang, S. Zhao, X. Lu, L. Yu, T. Mei and L. Zeng, *RSC Adv.*, 2014, **4**, 22009–22012.

3 J. Chen, S. Sun, C.-Z. Li, Y.-G. Zhu and B. P. Rosen, *Environ. Sci. Technol.*, 2013, **48**, 1141–1147.
4 J. Huang, X. Gao, J. Jia, J.-K. Kim and Z. Li, *Anal. Chem.*, 2014, **86**, 3209–3215.
5 X. Zhang, K. Xiao, L. Cheng, H. Chen, B. Liu, S. Zhang and J. Kong, *Anal. Chem.*, 2014, **86**, 5567–5572.
6 I. Al-Ogaidi, H. Gou, Z. P. Aguilar, S. Guo, A. K. Melconian, A. K. A. Al-kazaz, F. Meng and N. Wu, *Chem. Commun.*, 2014, **50**, 1344–1346.
7 L.-S. Huang, Y. Pheanpanitporn, Y.-K. Yen, K.-F. Chang, L.-Y. Lin and D.-M. Lai, *Biosens. Bioelectron.*, 2014, **59**, 233–238.
8 P. Phukon, K. Radhapyari, B. K. Konwar and R. Khan, *Mater. Sci. Eng., C*, 2014, **37**, 314–320.
9 R. de La Rica and M. M. Stevens, *Nat. Nanotechnol.*, 2012, **7**, 821–824.
10 F. Tanaka, *Chem. Rev.*, 2002, **102**, 4885–4906.
11 G. S. Wilson and Y. Hu, *Chem. Rev.*, 2000, **100**, 2693–2704.
12 J. T. Holland, C. Lau, S. Brozik, P. Atanassov and S. Banta, *J. Am. Chem. Soc.*, 2011, **133**, 19262–19265.
13 B. R. Baker, R. Y. Lai, M. S. Wood, E. H. Doctor, A. J. Heeger and K. W. Plaxco, *J. Am. Chem. Soc.*, 2006, **128**, 3138–3139.
14 J. Liu, Z. Cao and Y. Lu, *Chem. Rev.*, 2009, **109**, 1948–1998.
15 Y. Li, Y. Li, M. Hong, Q. Bin, Z. Lin, Z. Lin, Z. Cai and G. Chen, *Biosens. Bioelectron.*, 2013, **42**, 612–617.
16 T. Chen, M. Shao, H. Xu, S. Zhuo, S. Liu and S.-T. Lee, *J. Mater. Chem.*, 2012, **22**, 3990–3996.
17 D. Kriz and K. Mosbach, *Anal. Chim. Acta*, 1995, **300**, 71–75.
18 D. Cai, L. Ren, H. Zhao, C. Xu, L. Zhang, Y. Yu, H. Wang, Y. Lan, M. F. Roberts and J. H. Chuang, *Nat. Nanotechnol.*, 2010, **5**, 597–601.
19 X. Kan, Z. Xing, A. Zhu, Z. Zhao, G. Xu, C. Li and H. Zhou, *Sens. Actuators, B*, 2012, **168**, 395–401.
20 K. Haupt, *Chem. Commun.*, 2003, 171–178.
21 C. Malitesta, E. Mazzotta, R. A. Picca, A. Poma, I. Chianella and S. A. Piletsky, *Anal. Bioanal. Chem.*, 2012, **402**, 1827–1846.
22 K. Haupt and K. Mosbach, *Chem. Rev.*, 2000, **100**, 2495–2504.
23 K. Haupt, *Anal. Chem.*, 2003, **75**, 376A–383A.
24 B. Deore, Z. Chen and T. Nagaoka, *Anal. Chem.*, 2000, **72**, 3989–3994.
25 A. Mehdinia, M. O. Aziz-Zanjani, M. Ahmadifar and A. Jabbari, *Biosens. Bioelectron.*, 2013, **39**, 88–93.
26 D. Lakshmi, A. Bossi, M. J. Whitcombe, I. Chianella, S. A. Fowler, S. Subrahmanyam, E. V. Piletska and S. A. Piletsky, *Anal. Chem.*, 2009, **81**, 3576–3584.
27 F. Berti, S. Todros, D. Lakshmi, M. J. Whitcombe, I. Chianella, M. Ferroni, S. A. Piletsky, A. P. Turner and G. Marrazza, *Biosens. Bioelectron.*, 2010, **26**, 497–503.
28 B. Zhang, Y. Xu, Y. Zheng, L. Dai, M. Zhang, J. Yang, Y. Chen, X. Chen and J. Zhou, *Nanoscale Res. Lett.*, 2011, **6**, 431.
29 C.-L. Choong, J. S. Bendall and W. I. Milne, *Biosens. Bioelectron.*, 2009, **25**, 652–656.
30 I. Tokareva, I. Tokarev, S. Minko, E. Hutter and J. H. Fendler, *Chem. Commun.*, 2006, 3343–3345.
31 C. Xie, H. Li, S. Li, J. Wu and Z. Zhang, *Anal. Chem.*, 2009, **82**, 241–249.
32 H.-H. Yang, S.-Q. Zhang, F. Tan, Z.-X. Zhuang and X.-R. Wang, *J. Am. Chem. Soc.*, 2005, **127**, 1378–1379.
33 C. Sarkar, B. Basu, D. Chakroborty, P. S. Dasgupta and S. Basu, *Brain, Behav., Immun.*, 2010, **24**, 525–528.
34 S. E. Hyman and R. C. Malenka, *Nat. Rev. Neurosci.*, 2001, **2**, 695–703.
35 C. W. Olanow, O. Rascol, R. Hauser, P. D. Feigin, J. Jankovic, A. Lang, W. Langston, E. Melamed, W. Poewe and F. Stocchi, *N. Engl. J. Med.*, 2009, **361**, 1268–1278.
36 J. R. Berger, M. Kumar, A. Kumar, J. B. Fernandez and B. Levin, *AIDS*, 1994, **8**, 67–72.
37 J. R. Berger and G. Arendt, *J. Psychopharmacol.*, 2000, **14**, 214–221.
38 M. Tijero, G. Gabriel, J. Caro, A. Altuna, R. Hernández, R. Villa, J. Berganzo, F. Blanco, R. Salido and L. Fernández, *Biosens. Bioelectron.*, 2009, **24**, 2410–2416.
39 D. Pradhan, F. Niroui and K. Leung, *ACS Appl. Mater. Interfaces*, 2010, **2**, 2409–2412.
40 A. Singh, Z. Salmi, N. Joshi, P. Jha, A. Kumar, H. Lecoq, S. Lau, M. M. Chehimi, D. K. Aswal and S. K. Gupta, *RSC Adv.*, 2013, **3**, 5506–5523.
41 Y.-L. Chen, C.-Y. Lee and H.-T. Chiu, *J. Mater. Chem. B*, 2013, **1**, 186–193.
42 M.-S. Hsu, Y.-L. Chen, C.-Y. Lee and H.-T. Chiu, *ACS Appl. Mater. Interfaces*, 2012, **4**, 5570–5575.
43 X. Kan, H. Zhou, C. Li, A. Zhu, Z. Xing and Z. Zhao, *Electrochim. Acta*, 2012, **63**, 69–75.
44 S. P. Kounaves, *Handbook of Instrumental Techniques for Analytical Chemistry*, ed. F. A. Settle, Prentice Hall, New Jersey, 1997, ch. 37, pp. 709–726.
45 N. Maouche, M. Guergouri, S. Gam-Derouich, M. Jouini, B. Nessark and M. M. Chehimi, *J. Electroanal. Chem.*, 2012, **685**, 21–27.
46 L. Özcan, M. Sahin and Y. Sahin, *Sensors*, 2008, **8**, 5792–5805.
47 T.-C. Tsai, H.-Z. Han, C.-C. Cheng, L.-C. Chen, H.-C. Chang and J.-J. J. Chen, *Sens. Actuators, B*, 2012, **171–172**, 93–101.
48 B. Zhang, Y. Xu, Y. Zheng, L. Dai, M. Zhang, J. Yang, Y. Chen, X. Chen and J. Zhou, *Nanoscale Res. Lett.*, 2011, **6**, 1–9.
49 Y. Mao, Y. Bao, S. Gan, F. Li and L. Niu, *Biosens. Bioelectron.*, 2011, **28**, 291–297.
50 Y. Zeng, Y. Zhou, L. Kong, T. Zhou and G. Shi, *Biosens. Bioelectron.*, 2013, **45**, 25–33.
51 N. Gao, Z. Xu, F. Wang and S. Dong, *Electroanalysis*, 2007, **19**, 1655–1660.
52 W. Song, Y. Chen, J. Xu, X.-R. Yang and D.-B. Tian, *J. Solid State Electrochem.*, 2010, **14**, 1909–1914.
53 S. Gam-Derouich, M. Jouini, D. Ben Hassen-Chehimi and M. M. Chehimi, *Electrochim. Acta*, 2012, **73**, 45–52.

 